J Stat Phys (2011) 142: 1353–1370
DOI 10.1007/s10955-011-0172-4

Scaling of Linking and Writhing Numbers for Spherically Confined and Topologically Equilibrated Flexible Polymers

John F. Marko

Received: 2 November 2010 / Accepted: 2 March 2011 / Published online: 17 March 2011

Abstract Scaling laws for Gauss linking number Ca and writhing number Wr for spherically confined flexible polymers with thermally fluctuating topology are analyzed. For ideal (phantom) polymers each of N segments of length unity confined to a spherical pore of radius R there are two scaling regimes: for sufficiently weak confinement ($R \gg N^{1/3}$) each chain has $|\mathrm{Wr}| \approx N^{1/2}$, and each pair of chains has average $|\mathrm{Ca}| \approx N/R^{3/2}$; alternately for sufficiently tight confinement ($N^{1/3} \gg R$), $|\mathrm{Wr}| \approx |\mathrm{Ca}| \approx N/R^{3/2}$. Adding segment-segment avoidance modifies this result: for n chains with excluded volume interactions $|\mathrm{Ca}| \approx (N/n)^{1/2} f(\phi)$ where f is a scaling function that depends approximately linearly on the segment concentration $\phi = nN/R^3$. Scaling results for writhe are used to estimate the maximum writhe of a polymer; this is demonstrated to be realizable through a writhing instability that occurs for a polymer which is able to change knotting topology and which is subject to an applied torque. Finally, scaling results for linking are used to estimate bounds on the entanglement complexity of long chromosomal DNA molecules inside cells, and to show how "lengthwise" chromosome condensation can suppress DNA entanglement.

Keywords Polymer topology · Confined polymers · Polymer statistics · Chromosome structure · Chromosome topology

1 Introduction

Polymer physics consists in part in analysis of geometric constraints on molecule conformations, for example effects of chain flexibility, excluded volume, or confinement. However, topological constraints also play a major role in determining physical properties of polymers, particularly dynamical properties of dense, entangled chains [1, 2]. By contrast

J.F. Marko (✉)
Department of Physics and Astronomy and Department of Molecular Biosciences,
Northwestern University, Evanston, IL 60208, USA
e-mail: john-marko@northwestern.edu

with geometry, methods for study of topological constraint and entanglement are less well developed, and many basic problems concerning the topological properties of flexible polymers have not been analyzed. An area where such problems are of particular interest is that of chromosome dynamics, since mm or even cm-long DNA molecules must be replicated and physically separated during the process of cell division [3–8]. For consideration of DNA topology *in vivo*, the ensemble of fluctuating topology is relevant since topoisomerases (DNA-topology-changing enzymes) are present in large numbers [9, 10].

A basic problem of polymer topology is determination of the equilibrium distribution of linking topologies for two circular polymers. In this paper the topological quantity of interest is Gauss' linking number of two circular chains with contours described by space curves C and C' traced out by vectors $\mathbf{r}(n)$ and $\mathbf{r}'(n')$,

$$\mathrm{Ca} = \frac{1}{4\pi} \oint_C \oint_{C'} \frac{d\mathbf{r} \times d\mathbf{r}' \cdot (\mathbf{r} - \mathbf{r}')}{|\mathbf{r} - \mathbf{r}'|^3} \tag{1}$$

This paper uses the biophysical notation of "catenation number" Ca to refer to the Gauss linking number of two circular polymers.

The Gauss linking number Ca simply counts the total number of signed crossings of the two circular curves $\mathbf{r}$ and $\mathbf{r}'$. It is highly degenerate in the sense that many topologically distinct links take on the same value of Ca (e.g., all links with the same number of $+$ and $-$ crossings have $\mathrm{Ca} = 0$, the same linking number of the "unlink"), and therefore Ca is a poor choice for use as a precise topological classifier of specific links [11, 12].

Despite this, in many problems of polymer physics, one is less concerned with specifying a specific chain topology, than with determining whether two polymers are more or less entangled together under some particular conditions [13–15]. In the latter case, the distribution of Ca is a useful tool for determination of degree of entanglement. Given the signed nature of Ca, for the achiral polymers of interest here, in most cases $\langle \mathrm{Ca} \rangle = 0$. The focus in this paper will be on the linking number distribution width $\langle \mathrm{Ca}^2 \rangle$; the typical value of Ca can be estimated as $|\mathrm{Ca}| \approx \langle \mathrm{Ca}^2 \rangle^{1/2}$. Polymers with $\langle \mathrm{Ca}^2 \rangle \gg 1$ are highly entangled, while polymers with $\langle \mathrm{Ca}^2 \rangle \ll 1$ are essentially completely disentangled [15].

A result that will be important to this paper is $\langle \mathrm{Ca}^2 \rangle$ for two ideal circular polymers each of N segments which are constrained to share the same volume, (e.g., by being tethered together at a point along their contours [15]). For an ideal (phantom) polymer, the Gauss linking number (Ca) of two adjacent circular polymers scales as $|\mathrm{Ca}| \approx N^{1/4}$ [15], a scaling law first determined by Tanaka [16, 17]. Remarkably, introduction of excluded volume interactions dramatically suppresses equilibrium topology fluctuations in this problem to $|\mathrm{Ca}| \approx (\ln N)^{1/2}$ [15]. This effect of excluded volume interactions on chain topology is far stronger than the small shift of chain radius scaling from $\approx N^{1/2}$ for ideal polymers to $\approx N^{0.6}$ for polymers with excluded volume interactions, and is a consequence of segment correlations which lead to a long-range suppression of inter- and intrachain contacts [18, 19].

A quantity closely related to Ca is the "writhe" (Wr) of individual polymers [20]. Wr is a geometrical quantity which measures chirality of polymer fluctuations, and corresponds to the right-hand side of (1) but where $C = C'$, i.e., the Gauss formula evaluated for the *same* curve. Wr is not a topological property, but is a geometrical measure of chiral bending of one polymer.

In this paper the scaling of Ca and Wr are analyzed for n flexible circular polymers each N statistical segments in length, confined to a spherical cavity of radius R. The effect of confinement is to increase the degree of entanglement of the polymers, and at the same time to increase their writhes. A few workers have examined Ca [21, 22] and Wr [22–24]

distributions for confined polymers, but the present paper is the first to show how scaling laws unify results for wide ranges of R and N for ideal and self/mutually-avoiding polymers.

Section 2 analyzes Wr and Ca of chains of N unit-length segments confined to a spherical cavity of radius R. First, the scaling of Ca and Wr are discussed for noninteracting (phantom) polymers in a sphere: for both large- and small-chain limits, $|\mathrm{Ca}| \approx N/R^{3/2}$ on average for any pair of chains. For Wr, two distinct regimes exist depending on whether N/R^3, the scaling variable describing confinement, is small or large. For weak confinement, the well-known isolated-chain scaling law $|\mathrm{Wr}| \approx N^{1/2}$ applies, but for strong confinement, $|\mathrm{Wr}| \approx N/R^{3/2}$.

These scaling laws are then generalized to the case of polymers with excluded volume interactions, in dense melt and semi-dilute conditions. The change in the scaling laws are relatively minor modifications of those of noninteracting chains; the main change is that the regime where Wr increases as R is decreased is not physically accessible for polymers with appreciable self-avoidance, leading to the result that $|\mathrm{Wr}| \approx N^{1/2}$ under almost all circumstances. Wr scaling behaviors noted previously [23, 24] are consistent with the Wr scaling laws established here.

In Sect. 3 an application of the methods for estimation of Wr fluctuations is used to estimate the maximum Wr possible for a single tightly folded polymer. For ideal random walks it is argued that it is possible to find a state for which $\mathrm{Wr} \approx N^2$, and that this introduces the possibility of a writhing instability for a polymer where Wr is driven by a field, as discussed by Moroz and Kamien [25]. Numerical evidence is presented in favor of this scenario for ideal and self-avoiding polymers.

Finally Sect. 4 briefly discusses applications of the results of the paper to segregation of chromosomes, highlighting the efficacy of "lengthwise condensation" [6, 15] in driving entanglement removal even for highly confined polymers able to change their topology.

2 Catenation and Writhe Scaling for Spherically Confined Polymers

2.1 Ideal Polymers

Consider ideal, flexible "phantom" (noninteracting) circular polymers each of N monomers confined to a spherical cavity of radius R, with freely fluctuating topology. Outside the confining sphere, the polymers have a size $\approx N^{1/2}$. In the confined case, there are two scaling regimes; if the chains are sufficiently short, they fit inside the sphere (Fig. 1(a)). Alternately, for long chains, the chains have to "reflect" back and forth inside the sphere; since one crossing of the sphere requires R^2 monomers, there are N/R^2 "reflections" per chain (Fig. 1(b)).

2.1.1 Catenation Fluctuations

To estimate the Ca of two phantom chains, one should determine the number of "close encounters" of segments, since at those points one can change the sign of a crossing with no perturbation of the large-scale conformation of the chains [15]. Such exchanges can be made at each close encounter independently, so one obtains an estimate for Ca^2 equal to the number of close encounters.

(i) *Long chains:* $N^{1/2} > R$. For long chains which cross the sphere many times, the number of segment close encounters will be just N times the concentration of segments

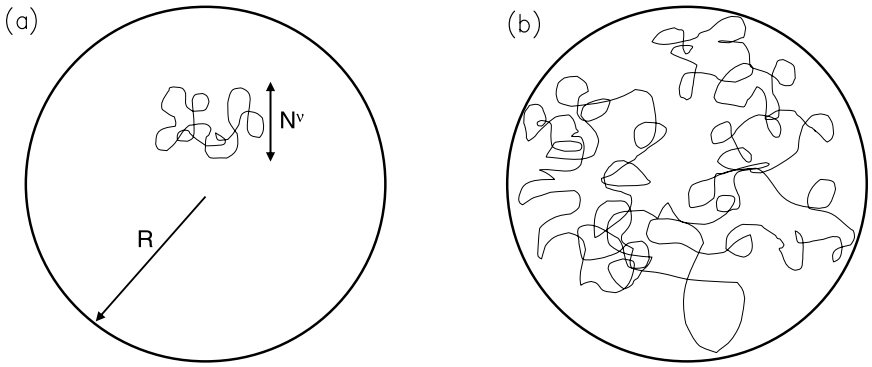

Fig. 1 A circular polymer of N segments confined within a sphere of radius R. (**a**) If the polymer is sufficiently short that its size $\approx N^{\nu} < R$ ($\nu = 1/2$ for ideal polymers, $\nu = 3/5$ for "good solvent" conditions), the polymer conformations are unperturbed by confinement. (**b**) If the polymer is long enough that $N^{\nu} > R$, then it must "reflect" from the wall of the confining sphere once per every $\approx R^{1/\nu}$ monomers. These two regimes apply not only to ideal polymers, but also describe the shapes of single chains in a polymer melt, or the conformations of strings of correlation "blobs" under semi-dilute solution conditions

contributed by the other chain (N/R^3), for a total of N^2/R^3. All chains are equally linked with all other chains, since they all cross the sphere multiple times.

(ii) *Short chains:* $N^{1/2} < R$. For short chains, for most configurations two given chains do not overlap. However, when two chains do happen to overlap, their catenation will be $\langle \mathrm{Ca} \rangle_{\mathrm{neighbor}} = N^{1/2}$ [15]. Now, the probability of the two phantom chains overlapping is proportional to the volume fraction occupied by either chain, i.e., $N^{3/2}/R^3$. Multiplying this by the linking-squared expected for neighbor chains together gives the estimate of the average linking-squared of two phantom chains averaged over all configurations, $\langle \mathrm{Ca}^2 \rangle \approx N^2/R^3$, the same result as for long chains.

2.1.2 Writhe Fluctuations

Wr for a chain counts its signed self-crossings, which scale differently for short and long chains. The reason for this is that there are two types of self-contacts, local and nonlocal. Local contacts occur every few segments due to small loops along the chains. They are randomly signed, and their total number scales with N, leading to the well-known result that $\mathrm{Wr}^2 \approx N$ for almost any kind of flexible polymer (ideal or good solvent) [21]; the same result holds for short enough chains confined to a sphere.

However, for sufficiently long chains in a sphere, there are additional self-contacts due to the chain crossing back and forth; again multiplying N monomers times the segment concentration N/R^3 one obtains a nonlocal contact Wr^2 contribution $\approx N^2/R^3$. The nonlocal contacts dominate Wr^2 only when $N^2/R^3 > N$, i.e., for $N > R^3$, or for $N^{1/3} > R$. Notably the polymer length at which the Wr scaling changes ($N \approx R^3$) is *larger* than the chain length at which the chain fills the sphere and starts to "reflect" from the walls of the cavity ($N \approx R^2$). It is to be emphasized that the regime where nonlocal contacts dominate and where $\langle \mathrm{Wr}^2 \rangle \approx N^2/R^3$ occurs for segment concentrations $N/R^3 > 1$.

2.1.3 Scaling Laws

Therefore, one may conclude that for phantom chains of N segments confined to a sphere of radius R,

$$\langle \mathrm{Ca}^2 \rangle \approx N^2/R^3$$
$$\langle \mathrm{Wr}^2 \rangle \approx \begin{cases} N & N/R^3 < 1 \\ N^2/R^3 & N/R^3 > 1 \end{cases} \tag{2}$$

This suggests a scaling function description of Ca and Wr fluctuations:

$$\langle \mathrm{Ca}^2 \rangle = N c(N/R^3)$$
$$\langle \mathrm{Wr}^2 \rangle = N w(N/R^3) \tag{3}$$

where $c(x)$ and $w(x)$ are functions with forms independent of N and R in the limit of large N and R. The catenation scaling function $c(x) \approx x$ for both small and large x, possibly with different prefactors in those two limits. The writhe scaling function has two different behaviors for small and large x; $w(x) \to a$ for $x \ll 1$, while $w(x) \to bx$ for $x \gg 1$, for some $\mathcal{O}(1)$ constants a and b. The forms (3) indicate that both $\langle \mathrm{Ca}^2 \rangle$ and $\langle \mathrm{Wr}^2 \rangle$ are extensive in N, times a scaling function dependent only on the segment concentration.

2.1.4 Numerical Test of Scaling Laws

A numerical test of (3) is indicated. Figure 2 shows plots of $\langle \mathrm{Ca}^2 \rangle/N$ and $\langle \mathrm{Wr}^2 \rangle/N$ versus N/R^3 for a number of values of N and R, for Monte Carlo simulations of two circular freely-jointed ideal polymers (closed "phantom" polygons with no self- or mutual-segment avoidance) confined in a spherical cavity of radius R. The segment lengths were allowed to fluctuate between 0.9 and 1.1 units of length, and single-vertex "diffusion" and random-length crankshaft-rotation moves were used to equilibrate the chains (for details see [15]). Five independent runs were used to obtain statistics for each (N, R) case, each roughly 10^6 Monte-Carlo steps per monomer in length. It was verified that each run was many correlation lengths long, and error bars were calculated from the variance of averaged quantities for the different runs.

Results are shown in Fig. 2 for a number of (N, R) pairs: $R = 4$ ($\diamond$) for $N = 320$, 640 and 1280; $R = 4.5$ (Δ) for $N = 1280$; $R = 6$ ($+$) for $N = 1280$; $R = 8$ ($\circ$) for $N = 80$, 160, 320, 640 and 1280; $R = 16$ ($\square$) for $N = 80$, 160, 320, 640 and 1280; $R = 24$ ($*$) for $N = 320$ and 640; $R = 32$ ($\times$) for $N = 320$ and 640; and $R = 40$ (∇) for $N = 640$. In Fig. 2(a) $\langle \mathrm{Ca}^2 \rangle/N$ is plotted as a function of N/R^3, in accord with (3); the data collapse onto a single curve, indicating that the scaling argument is in accord with the numerical data. Furthermore, the data fall onto a nearly linear curve: the solid line in Fig. 2(a) is $\langle \mathrm{Ca}^2 \rangle/N = 0.04067 N/R^3$. The small- and large-$N/R^3$ limits of the scaling function appear to have slightly different prefactors, but both limits are well described by (3).

Figure 2(b) shows $\langle \mathrm{Wr}^2 \rangle/N$ for the same MC data set; the same symbols are plotted for the various (N, R) cases as in Fig. 2(a). In accord with (3), the data collapse onto a scaling function which goes to a constant $\mathcal{O}(1)$ limit for small N/R^3, and which becomes approximately linear in N/R^3 for large values of that variable. The solid curve in Fig. 2(b) is $\langle \mathrm{Wr}^2 \rangle = [0.14^{1.125} + (0.08x)^{1.125}]^{1/1.125}$ where $x = N/R^3$, which has the small- and large-x limits described in (3). The collapse of the numerical data thus indicates that the scaling laws of (2) and (3) hold with the expected asymptotic behaviors of the scaling functions.

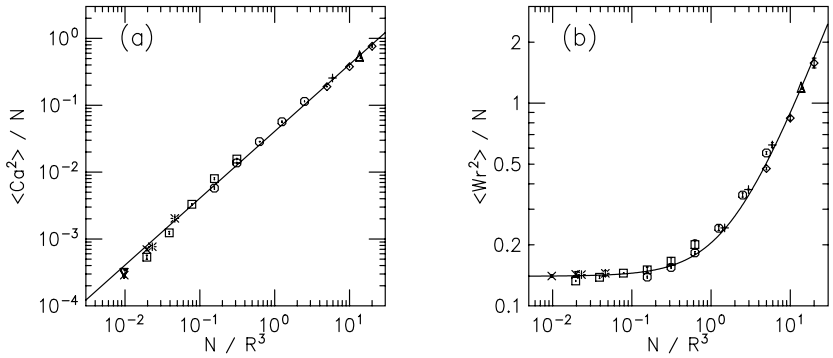

Fig. 2 Scaling behavior of catenation and writhe fluctuations for phantom polymers of N unit-length segments confined to a sphere of radius R. (**a**) Catenation $\langle \mathrm{Ca}^2 \rangle / N$ scales linearly with the variable $x = N/R^3$ for both small and large x (*solid line* is $\propto x$, see text). (**b**) Writhe $\langle \mathrm{Wr}^2 \rangle / N$ goes to a constant limit as $x \ll 1$, and approaches the limit $\sim x$ for $x \gg 1$. *Solid curve* is a fit scaling function that goes to a constant for small x and behaves linearly for large x (see text)

2.2 Polymers with Excluded-Volume Interactions

2.2.1 Melt Conditions

Now consider the more realistic case of n circular polymers each of N segments confined in a sphere of radius R, where the segments have excluded-volume interactions with one another. It is instructive to first consider the limit of i.e., where the segment density, nN/R^3, is a constant (one can imagine the volume fraction to be unity). In this case segment correlations are screened at scales larger than the statistical segment length (taken to be unity here) so the polymer statistics are IRW (Gaussian) at scales smaller than the pore radius R, and the chain conformation at larger scales undergoes "reflection" from the pore walls, just as in the previous subsection (Fig. 1).

The volume occupied by the segments is $nN = R^3$, or $R = n^{1/3}N^{1/3}$; by applying this constraint to the results of the previous subsection the scaling properties for the melt are obtained:

$$\begin{aligned} \langle \mathrm{Ca}^2 \rangle &= \frac{N^2}{R^3} = \frac{N}{n} \\ \langle \mathrm{Wr}^2 \rangle &= N \end{aligned} \tag{4}$$

Note that $N \leq R^3$ always holds for a melt of $n > 1$ chains.

These scaling laws hold in both the limits of short ($N^{1/2} < R$, or $n > N^{1/2}$) and long ($N^{1/2} > R$, equivalently $n < N^{1/2}$) chains, and have simple physical interpretations. When overfilling of space is suppressed by the melt volume constraint, Wr is dominated by random signs contributed by the $\sim N$ small loops along each polymer length. On the other hand, since Ca counts interchain crossings, in the melt there is ~ 1 crossing per segment. Only $1/n$ of those are contributed by a given neighbor chain, giving $\mathrm{Ca}^2 \sim N/n$ for any two chains in the pore.

In the case of short chains $N^{1/2} < n$, $\langle \mathrm{Ca}^2 \rangle = N/n$ continues to be true for any two chains averaged over all conformations, but for short chains, each conformation consists of chains

which are spatially isolated from many of the other chains. For the melt, each chain in each configuration interacts with only $N^{1/2} < n$ neighbor chains and has catenation

$$\langle \mathrm{Ca}^2 \rangle_{\mathrm{neighbor}} = N^{1/2} \tag{5}$$

with each of those neighbors. The short-chain melt case illustrates the possibility for a difference between linking of a chain with its neighbor chains ($\langle \mathrm{Ca}^2 \rangle_{\mathrm{neighbor}}$), and the linking of two particular chains averaged over all configurations ($\langle \mathrm{Ca}^2 \rangle$). For the short-chain melt, the *total* number of catenations of one chain with its $N^{1/2}$ neighbors is therefore $\propto N$, in accord with previous estimates [26–29].

The same scaling laws will hold for a collapsed globule formed by n polymers of N segments each adhered together under poor solvent conditions, assuming equilibration of topology.

2.2.2 *Semi-dilute Conditions*

The results of the previous subsection may be generalized to the case where the polymers are less crowded. If the polymers are put into the pore at a concentration below that where space is filled in the presence of a "good solvent" in which the segments do not adhere to one another, then the polymers will form a droplet of semi-dilute solution (SDS) of segment concentration nN/R^3. The polymers will have self-avoiding walk (SAW) statistics in the absence of confinement, and therefore the unperturbed size of a chain of N monomers is N^{ν}. The condition that one has sufficient overlap of the chains to generate a SDS is simply $nN^{3\nu} > R^3$. Combining this with the condition that the concentration be less than the melt case gives the range for SDS behavior, $N^{1/3} < R/n^{1/3} < N^{\nu}$. For three dimensions recall that the exponent is close to the Flory value $\nu = 3/5$, so for reasonable values of N, the range of R for which there is SDS behavior is narrow.

In the semi-dilute case, the structure of the droplet is that of a melt of SDS correlation "blobs" containing monomers from just one of the polymers. If the blob size is ξ and the number of monomers in a blob is g, then $\xi = g^{\nu}$, and the concentration must satisfy $nN/R^3 = g/\xi^3$. Solving these two equations gives $g = R^{3/(3\nu-1)}/(nN)^{1/(3\nu-1)} = 1/\phi^{1/(3\nu-1)}$ as the number of monomers per blob, where the final expression is in terms of the segment concentration $\phi \equiv nN/R^3$.

The average Ca^2 follows from (4) via replacement of N with the number of blobs per chain, N/g:

$$\langle \mathrm{Ca}^2 \rangle \approx \frac{N}{n} \phi^{1/(3\nu-1)} \approx \frac{N}{n} \phi^{5/4} \tag{6}$$

where the final term plugs in the Flory exponent $\nu = 3/5$, and where the segment concentration $\phi = nN/R^3$ has been used. Because of the variation in blob size with concentration, there are slightly stronger N and R dependences than found for the ideal random walk but overall the scaling behavior is only slightly modified from the melt case. In the melt limit $\phi \to 1$ one recovers the melt result (4).

Equation (6) assumes that each blob crossing contributes unity to $\langle \mathrm{Ca}^2 \rangle$, which is not quite complete, since two adjacent SAWs each of g monomers have $\langle \mathrm{Ca}^2 \rangle \approx \ln g$ [15], and therefore exchange of two adjacent blobs will change $\langle \mathrm{Ca}^2 \rangle$ by this amount. Therefore there is a blob-blob catenation correction to (6) (the formula should include a leading $\ln g$). This weak correction does not change the power-law scaling, and is not likely to be observable.

For the short-chain case ($[N/g]^{1/2} < n$) one can estimate the number of links a chain has with its neighbors in any configuration. Each chain overlaps with $(N/g)^{1/2} = N^{1/2}\phi^{1/[2(3\nu-1)]}$ other chains, and has $\mathrm{Ca}^2 = (N/g)^{1/2}$ with each of those chains, or

$$\langle \mathrm{Ca}^2 \rangle_{\mathrm{neighbor}} = N^{1/2}\phi^{1/[2(3\nu-1)]} = \frac{n^{1/[2(3\nu-1)]}N^{3\nu/[2(3\nu-1)]}}{R^{3/[2(3\nu-1)]}} = \frac{n^{5/8}N^{9/8}}{R^{15/8}} \tag{7}$$

where the last equation corresponds to use of the Flory exponent $\nu = 3/5$.

One is tempted to compute Wr^2 using the blob argument, but counting chain self-crossings at the blob scale will give a contribution $\sim N/g$ to Wr, which is much smaller than the $\sim N$ that will be contributed by small loops along the chain. Therefore the writhe will continue to scale as

$$\langle \mathrm{Wr}^2 \rangle \approx N \tag{8}$$

with an amplitude which will depend on segment concentration contributed by *one* chain, $\phi_1 = N/R^3 = \phi/n$.

2.2.3 Scaling Laws for Semi-dilute and Concentrated Solution

Results for overlapping chains at all segment concentrations (highly concentrated melt-like and SDS cases) can be summarized by one pair of scaling laws

$$\begin{aligned} \langle \mathrm{Ca}^2 \rangle &= \frac{N}{n}\, c(\phi) \\ \langle \mathrm{Wr}^2 \rangle &= N\, w(\phi_1) \end{aligned} \tag{9}$$

for scaling functions c and w that depend only on the segment density $\phi = nN/R^3$ and the one-chain segment density $\phi_1 = N/R^3$, respectively. The scaling function $c(\phi) \propto \phi^{1/(3\nu-1)} \approx \phi^{5/4}$ for $\phi \ll 1$; as ϕ approaches the melt limit ($\phi \approx 1$), this function should approach $c(\phi) \propto \phi$. On the other hand, the writhe scaling function $w(\phi_1)$ should remain $\mathcal{O}(1)$ for all ϕ, and is dependent on the single-chain density $\phi_1 = \phi/n$.

2.2.4 Numerical Test of Scaling Laws

Numerical calculations were carried out as in Sect. 2.1.4, following the procedure described in Ref. [15], for $n = 2$ or $n = 4$ polymers each of N monomers confined within a sphere of radius R. The polymer segments have a cylindrical shape, of unit length and cross-sectional diameter $d = 0.2$. The volume fraction occupied by polymer segments is $\eta = 3nd^2N/(16R^3)$; for $d = 0.2$ this becomes $\eta = (3/400)nN/R^3$. Since the maximum volume fraction allowed for packing of cylinders is $\eta = \pi/(2\sqrt{3}) = 0.9068\ldots$, the maximum numerical value of the segment density is $\phi = nN/R^3 = 200\pi/(3\sqrt{3}) \approx 121$. Again, five independent runs were carried out, each of between 10^6 and 10^7 Monte-Carlo steps per monomer. Errors were calculated from the run-to-run variances.

Results are shown in Fig. 3, where $\langle \mathrm{Ca}^2 \rangle/(N/n)$ is plotted as a function of segment concentration $\phi = nN/R^3$, and where $\langle \mathrm{Wr}^2 \rangle/N$ is plotted as a function of the one-chain density $\phi_1 = N/R^3$. The different data points show data for: $R = 4$ ($\diamond$) for $n = 2$ with $N = 160$ and 320; $R = 6$ ($+$) for $n = 2$ with $N = 320$ and 640; $R = 8$ ($\circ$) for $n = 2$ with $N = 160$, 320 and 640 and for $n = 4$ with $N = 160$ and 320; $R = 10$ ($*$) for $n = 2$ with $N = 160$ and 640; $R = 16$ ($\square$) for $n = 2$ with $N = 160$, 320 and 640; $R = 24$ ($\times$) for $n = 2$ and $N = 1280$; and $R = 30$ (∇) for $n = 2$ and $N = 1280$.

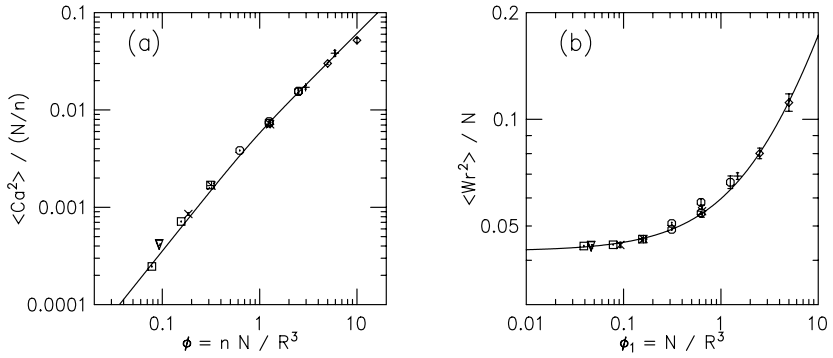

Fig. 3 Scaling behavior of catenation and writhe fluctuations for circular polymers of N unit-length segments confined to a sphere of R. The segments have a diameter 0.2 times their length and interact via excluded-volume interactions. (**a**) Catenation $\langle \mathrm{Ca}^2 \rangle / N$ scales linearly with the segment density $\phi = nN/R^3$ for $x > 1$, and faster than linearly for $\phi < 1$. *Solid curve* is a fit function that interpolates between the asymptotic behaviors $\phi^{5/4}$ and ϕ^1 expected for $\phi < 1$ and $\phi > 1$, respectively (see text). (**b**) Writhe $\langle \mathrm{Wr}^2 \rangle / N$ goes to a constant limit for $x_1 = N/R^3 \ll 1$; for $\phi_1 > 1$, there is a slight increase with x_1 similar to that seen in Fig. 2(b), but the extent of this increase is limited by the finite-density constraint imposed by segment-segment excluded volume interactions. *Solid curve* is a fit function that interpolates between the constant and $\approx \phi$ asymptotic behaviors expected for $\phi < 1$ and $\phi > 1$ (see text)

When plotted using the scaling variables of (9), the results collapse onto single curves. For low concentrations, the Ca graph (Fig. 3(a)) has a slope consistent with the expected SDS slope of 5/4; for larger concentrations the slope drops to near 1 expected for dense, melt-like systems where the range of segment correlation is short. The solid curve plotted through the data is $\langle \mathrm{Ca}^2 \rangle / N = 2(0.01x)^{5/4}/[1 + (1.15x)^{10/4}]^{1/10}$ for $x = nN/R^3$, which changes smoothly between $x^{5/4}$ and x dependence in small- and large-x limits.

The result for Wr/N is nearly constant ($\mathrm{Wr}^2 \sim N$) as expected, with a slight (less then threefold) increase of the scaling function with increasing single-chain segment density $\phi_1 = N/R^3$. The smooth curve shown in Fig. 3(b) is $\langle \mathrm{Wr}^2 \rangle = [0.0425^{0.83} + (0.011x)^{0.83}]^{1/0.83}$ and changes smoothly from constant for small $x = N/R^3$, to $\propto x$ for large x. In conclusion, numerical data for $\langle \mathrm{Ca}^2 \rangle$ and $\langle \mathrm{Wr}^2 \rangle$ are well described by the scaling behaviors of (9).

2.2.5 Isolated Self-avoiding Chains

If the spherical pore is large enough that the chains fit into it without overlapping, i.e., if $R > n^{1/3} N^{\nu}$, then the chains only overlap for a fraction $N^{3\nu}/R^3$ of all conformations. For each overlapping conformation, the chains will have $\mathrm{Ca}^2 \approx \ln N$ [15]. The average catenation of any two chains will therefore be

$$\langle \mathrm{Ca}^2 \rangle \approx \frac{N^{3\nu}}{R^3} \ln N = \frac{N^{9/5}}{R^3} \ln N \tag{10}$$

For isolated SAWs, $\langle \mathrm{Wr}^2 \rangle \approx N$.

3 Writhe Instability for a Single Polymer

3.1 Maximum Writhe of a Polymer

The analysis of Wr scaling in Sect. 2 suggests an estimate for the maximum possible value of Wr for a single phantom circular polymer. For phantom polymers under spherical confinement, $|\mathrm{Wr}| \approx N/R^{3/2}$, by a crossing-counting argument that was validated numerically. For phantom chains, or for chains with small excluded volume (e.g., semiflexible chains with a large segment length to diameter ratio, note that naked DNA has a ratio of about 20), one can imagine making the confinement radius comparable in size to one polymer segment, with the result that $|\mathrm{Wr}| \approx N$, much larger than the $\approx N^{1/2}$ writhe of an unconstrained polymer. This scaling has been observed for phantom polymers under extreme confinement in a volume of cross-sectional dimension comparable to a segment length [22].

In this extreme limit, there are N^2 crossings, i.e., every segment crosses all N other segments of the polymer in most viewing projections. The writhe is the square root of the number of crossings since they are randomly signed. However, by making all the crossings the same sign, one can imagine achieving

$$|\mathrm{Wr}|_{\mathrm{maximum}} \approx N^2 \tag{11}$$

for the writhe of a *chirally* collapsed or confined polymer. This value of Wr is the maximum possible: it requires correlated-sign crossings of every segment with every other segment in every projection.

In addition to the confinement free energy ($\approx Nk_BT$) there will be an additional free energy cost $\approx Nk_BT$ for generating the same-sign crossings since each segment must be specifically oriented to generate same-sign crossings. To achieve the maximally writhed state, the polymer will have to become highly chirally knotted, so there will have to be available mechanisms for knotting topology change (e.g., type-II topoisomerases for DNA molecules). The maximally-writhed state is distinct from the plectonemically supercoiled state, which has $|\mathrm{Wr}| \approx N$ and which is unknotted.

3.2 Writhe-Driven Chiral Collapse of a Polymer

The possibility of a $|\mathrm{Wr}| \approx N^2$ collapsed state suggests that there may a phenomenon of writhe-driven chiral polymer collapse that can be driven by a field coupled to polymer Wr. The most straightforward mechanism for driving Wr is the coupling of mechanical torque τ to the Lk of a polymer with twist rigidity (e.g., double-helix DNA). The energy function for this situation is

$$\frac{E}{k_BT} = E_{\mathrm{bend}} + \frac{2\pi C}{L}(\Delta\mathrm{Tw})^2 - 2\pi\tau\,\Delta\mathrm{Lk} \tag{12}$$

Here the conformational bending free energy depends only on the polymer shape $\mathbf{r}(s)$, and the twisting energy depends only on the total twist Tw. The Fuller-White formula $\Delta\mathrm{Lk} = \Delta\mathrm{Tw} + \mathrm{Wr}$ allows the final torque term to be decoupled into twist and writhe contributions, where Wr depends only on the polymer shape $\mathbf{r}(s)$. For this model, the fluctuations of ΔTw may be integrated out, leaving an effective free energy for the conformational fluctuations of the form

$$\frac{F}{k_BT} = E_{\mathrm{bend}} - 2\pi\tau\,\mathrm{Wr} + \mathrm{constant} \tag{13}$$

indicating that mechanical torque coupled to ΔLk amounts to a coupling of the torque to Wr. This direct coupling of torque to Wr in the presence of type-II topoisomerases able to change knotting state could lead to formation of a highly writhed state, but only if torsional stress was replenished faster (e.g., by rapid rotation of the end of a tethered polymer) than those same type-II topoisomerases were able to relax it.

3.3 Numerical Test for Ideal Polymers

As a test of the existence of the writhing instability proposed above, Monte Carlo simulations of single ideal polymer rings of N segments were carried out following the method of [15], but with the energy $\Delta E = -2\pi\tau\,\mathrm{Wr}$. The rings were sampled in equilibrium with fixed torque of $2\pi\tau = 1$ ($\tau = 0.1592$). Figure 4(a) shows representative collapsed conformations for $N = 20$, $N = 80$ and $N = 320$. The chains are folded back on themselves at every segment to form a compact conformation in which every segment can overlap the majority of the other segments. Writhes obtained as a function of polymer length N are shown in Fig. 4(b) ($\circ$). The collapsed chains have a writhe which scales as the square of chain length, well approximated by $\mathrm{Wr} = (N/1.65)^2$ (Fig. 4(b), solid line).

For one polymer length ($N = 80$), average Wr is shown as a function of the torque τ, in Fig. 4(c). These data were obtained from a series of simulations at gradually increased torque. The onset of the collapse is abrupt, and occurs for a critical torque value $2\pi\tau \approx 0.251$, where Wr jumps by approximately 100-fold. This first-order-like onset of tight writhing is in rough accord with the scenario described by Moroz and Kamien for a polymer subject to a field coupled to writhe [25].

Figure 4(d) shows the critical torque beyond which writhe collapse occurs as a function of chain length N, determined by gradually increasing the torque from zero, until collapse is observed (as in Fig. 4(c)). For small polymers more torque is needed than for large polymers, and for large N, the critical torque approaches a constant, $\mathcal{O}(1)$ value. The critical torque shown in Fig. 4(d) represents the limit of stability of the low-writhe ("chiral random polymer" [30]) state.

3.4 Effect of Excluded Volume Interactions

Given the dramatic behavior shown in Fig. 4(a)–(d) for ideal polymers, one would like to know whether a similar effect persists for chains of finite thickness. Figure 4(e) shows average Wr as a function of torque τ for a circular polymer with $N = 80$ segments and segment thickness $d = 0.05$ (a thickness to segment length ratio similar to that of naked double-stranded DNA in physiological buffer); again an abrupt collapse is observed, but for a larger torque ($2\pi\tau \approx 0.44$) than for the ideal polymer case (compare with Fig. 4(c)): more torque is needed to drive the now self-avoiding polymer near itself so as to generate large writhe.

Finally, data for the collapsed state writhe at a torque of $\tau = 0.1592$ for the $d = 0.05$ case are shown in Fig. 4(b) ($\times$), for various chain lengths. The writhe is below that of the ideal polymer case, but does follow $\mathrm{Wr} \approx N^2$ as in the ideal case for small chain lengths. However, beyond $N = 80$, the rate of increase of Wr with N drops. This is reasonable since at some N the tight configurations for ideal polymers (Fig. 4(a)) will become impossible to realize for finite-thickness polymers, so the collapsed polymer will have to start to elongate, suggesting a scaling behavior $\mathrm{Wr} \approx N$ with a numerically large prefactor. These data establish that the writhe instability analyzed in detail above for ideal polymers exists for self-avoiding polymers (for finite chain thickness).

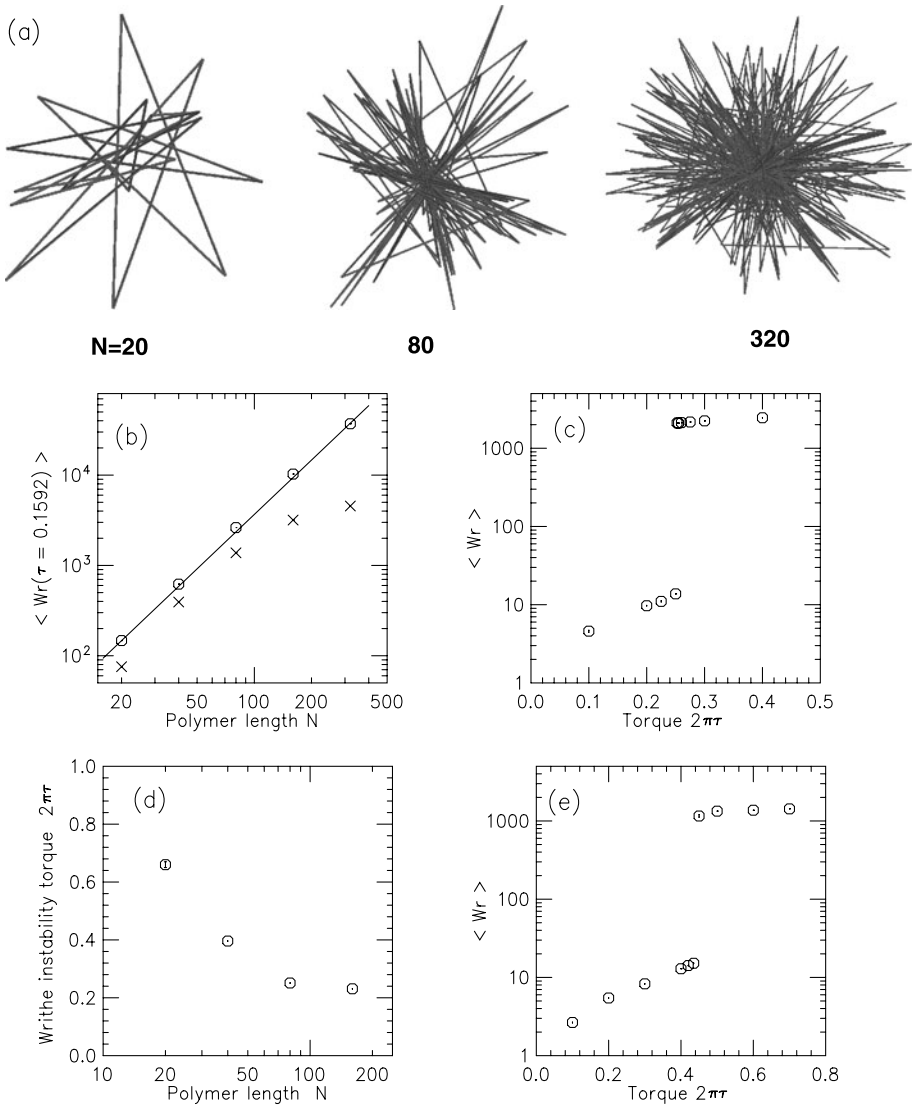

Fig. 4 Torque-driven writhing instability of a single ring polymer. (**a**) Typical writhe-collapsed polymer conformations for ideal (zero-thickness) polymers for $N = 20$, 40 and 320, for constant torque $\tau = 0.1592$. (**b**) Writhe versus polymer length N for $\tau = 0.1592$. Results are shown for ideal polymers with zero thickness ($\circ$), which closely follow $\mathrm{Wr} \approx (N/1.65)^2$ (*line*). Results for self-avoiding polymers are also shown ($\times$) for segment thickness $d = 0.05$. Excluded volume reduces the maximum Wr that can be attained, and for large enough N, changes the scaling behavior. (**c**) Onset of writhe instability for ideal (zero-thickness segment) polymers. Equilibrium Wr versus τ is plotted for a polymer of $N = 80$ segments. An abrupt transition is observed for $2\pi\tau \approx 0.251$. (**d**) Torque for onset of writhe instability as function of chain length N. (**e**) Onset of writhe instability for self avoiding polymer with $N = 80$ and segment thickness $d = 0.05$. There is still an abrupt transition to a collapsed high-Wr state, but at a larger value of torque ($2\pi\tau \approx 0.44$) than in the zero-thickness case (compare with (**b**))

4 Chromosome Entanglement and Segregation

4.1 Equilibrated Topology of Human Chromosomes

Given a scaling theory for equilibrium linking for confined polymers, one can estimate the thermal equilibrium entanglement using (9), $\langle Ca^2\rangle_0 = (N/n)c(nN/R^3)$, that would occur for otherwise unconstrained chromosomes within a cell nucleus, under the assumptions that random strand passages are made by type-II topoisomerases, and that the chromosomes behave as self-avoiding polymers.

A statistical segment of chromatin is thought to be roughly $b = 60$ nm in length, 30 nm wide, containing about 35 nucleosomes, or 6 Kb of DNA. Thus, the larger human chromosomes, approximately 200 Mbp in length, as chromatin correspond to $N \approx 30{,}000$ segment-long polymers. Human chromosomes are confined within a cell nucleus of radius $R \approx 3$ μm, or measured in polymer segment units, $R/b = 50$. The number of chromosomes in a human nucleus is $n = 46$, thus we can compute the segment density $\phi = nN/(R/b)^3 = 10$, corresponding to a volume fraction of roughly 10%. Reading off $\langle Ca^2\rangle/(N/n) = 0.06$ for this ϕ value from Fig. 3 gives the estimate $\langle Ca^2\rangle_0 = 40$. This is likely an overestimate since chromatin fiber has a segment diameter-to-length ratio larger than the $b/d = 0.2$ used to compute Fig. 3. In conclusion, if human chromosomes were to fully equilibrate their topology, they would be expected to have $\langle Ca^2\rangle \approx 40$; i.e., they would equilibrate to an entangled state. However, the value of $\langle Ca^2\rangle$ is much smaller than N in numerical size.

It is to be stressed that $\langle Ca^2\rangle_0$ is not necessarily the actual catenation that occurs in the cell, but only that which would occur if topology were equilibrated for uncondensed chromosomes in a nucleus. It has been estimated that the time needed for topological equilibrium may greatly exceed cell-cycle timescales, and that observations of chromosome territories (distinct spatial regions of the nucleus that contain separate chromosomes) may be related to this kinetic constraint [7]. Other factors such as tethering of chromosomes to the nuclear envelope during interphase [7], or formation of condensed heterochromatin domains, likely play a major role in maintaining chromosome territories and limiting chromosome entanglement. Nevertheless, the estimate $\langle Ca^2\rangle_0$ is useful as it is a thermodynamic upper bound on entanglement of chromosomes confined to a nucleus.

4.2 Topological Resolution of Chromosomes Driven by Lengthwise Condensation

During cell division, chromosomes become completely segregated from one another, despite the fact that following DNA replication, the chromosomes are released from being tethered to the inside of the nuclear envelope, and have an opportunity to entangle with one another. Evidence for inter-chromosome entanglements have been obtained from experiments in fission yeast where the DNA-topology-changing enzyme topo II was disabled during chromosome condensation: *different* chromosomes were observed to be unable to segregate from *one another* [31]. Similar effects have been observed *in vitro* in experiments with *Xenopus* egg extracts [32], and *in vivo* for mammalian cells [33, 34]. These observations of inter-chromosome entanglements following suppression of topo II activity imply that chromosomes became entangled with one another at some time prior to the inhibition.

Strikingly, following DNA replication, chromosomes start to *condense* into string-like structures that become gradually visible in the light microscope. This process of "chromosome condensation" is thought to be coupled to the process of segregation of chromosomes from one another [3, 5, 6] as well as to separation of sister chromatids from one another inside each chromosome (the focus here is less on the segregation of the duplicate sister

chromatids from one another [15], but rather on the segregation of different chromosomes). Below it will be argued that the peculiar type of condensation that occurs—"lengthwise condensation", or folding of chromosomes along their length—ensures separation of different chromosomes, provided that topo II is present during the condensation process.

Previously it was argued that lengthwise condensation can drive topological separation of two polymers that are tethered to one another [15]. The results of Sect. 2 allow one to see how lengthwise condensation can drive segregation of different chromosomes even while confined inside the nucleus. Consider chromosomes which are initially in the form of flexible polymers of N statistical segments each of b and cross-sectional diameter d. Suppose lengthwise condensation occurs: the chromosomes will become locally thicker ($d \to d' > d$), but in doing so will become stiffer ($b \to b' > b$) and shorter ($L = Nb \to L' = N'b' < N$). A simple and reasonable assumption is that the condensation process will conserve chromatin volume, i.e. $Ld^2 = L'd'^2$, or $Nbd^2 = N'b'd'^2$. To simplify the calculation to follow, it will be assumed that as condensation occurs, b and d will increase by the same factor, i.e., $b' = \lambda b$ and $d' = \lambda d$. For this particular model of chromosome condensation the volume conservation constraint indicates $N' = N/\lambda^3$. This simple model of chromosome condensation describes the degree of condensation by the single parameter $\lambda > 1$.

As chromosome condensation occurs, λ gradually increases, and by (9) the equilibrium catenation of chromosomes will be

$$\langle \mathrm{Ca}^2 \rangle_\lambda = \frac{N'}{n} c\left([nN'b'^3]/R^3\right) = \frac{1}{\lambda^3}\frac{N}{n} c\left([nNb^3]/R^3\right) = \frac{1}{\lambda^3}\langle \mathrm{Ca}^2 \rangle_0 \tag{14}$$

where $\langle \mathrm{Ca}^2 \rangle_0$ is the catenation that would be achieved in topological equilibrium *before* chromosome condensation begins (the estimate made above for human chromosomes). Note that the level of entanglement of chromosomes need not initially be close to $\langle \mathrm{Ca}^2 \rangle_0$ for (14) to apply during chromosome condensation. Equation (14) indicates the equilibrium catenation that can be reached, assuming random strand passages by topoisomerase II, given lengthwise condensation by a factor λ, and shows how lengthwise condensation can generate a strong thermodynamic drive to eliminate catenations between different chromosomes. The interactions that accomplish local condensation of chromosomes by a factor λ suppress the equilibrium level of entanglement $\langle \mathrm{Ca}^2 \rangle$ by a factor λ^{-3}.

Therefore, the equilibrium catenation expected for uncondensed human chromosomes, $\langle \mathrm{Ca}^2 \rangle = 40$, can be pushed well below 1 by only moderate condensation $\lambda = 6$. Therefore, by locally folding chromatin fiber from its uncondensed level (30 nm thickness) to a condensed 200 nm-thick fiber will ensure complete decatenation of different chromosomes. The increase of b and d by the same factor λ allows the same scaling function $c(\phi)$ to be used which simplifies this computation, but this condition is not required to obtain the same condensation-driven topological resolution. Finally, it should be noted that the segment density is unchanged by this condensation process, but the total number of segments per chain is reduced by a factor λ^3; for the human chromosome case considered above ($\lambda = 6$) $N' = N/\lambda^3 \approx 30,000/200 \approx 150$. Thus, when human chromosomes become separated by this process, they will still be relatively long, flexible polymers.

To summarize, the mechanism outlined here of lengthwise-condensation-driven entanglement removal requires that there first be enzymes which act to condense chromatin along its length, without introduction of "cross-links" between different chromosomes. Then, this condensation system must act slowly enough that there is time for topology-changing enzymes (topo II) to release entanglements between different chromosomes. Given these two requirements, as lengthwise condensation goes forward, entanglements will be

released at successively large length scales by the combined action of the lengthwise-condensation mechanism and topo II. In accord with this, disturbing either the condensation or topology-changing machinery has been observed to disrupt the condensation-resolution process [31–36]. Finally, fully condensed chromosomes become "individualized" (lengthwise condensation can generate this as well, see Ref. [15]), and following separation of sister chromatids, the two sets of replicated chromosomes then decondense to form nuclei. As emphasized by Rosa and Everaers [7] kinetic effects may delay full re-entanglement, giving time for establishment of chromosome tethering and other nuclear structures factors stabilizing chromosome territories.

4.3 Estimates for Bacterial Chromosomes

Bacterial chromosomal DNAs ($\approx 5 \times 10^6$ bp) are much shorter than those of humans, but bacteria also do not have histones and chromatin fiber. Instead bacterial chromosomes are compacted at the lowest level by the action of DNA-bending proteins [37]. The result is that a single statistical segment of bacterial chromosome likely contains $\approx 5 \times 10^2$ bp and has $b \approx 50$ nm. The result is $N \approx 10^4$, similar to the value for human chromosomes despite the latter's much larger length. The size of bacterial cells is $R \approx 500$ nm. So, considering the situation where following DNA replication during slow growth there are $n = 2$ chromosomes in a bacterial cell, $\phi = nN/(R/b)^3 = 20$, giving $c(\phi) \approx 0.1$ (see Fig. 3). Thus, for bacterial chromosomes confined to a bacterial cell, $\langle \mathrm{Ca}^2 \rangle_0 \approx (N/n)c(\phi) \approx 10^3$. Chromosomes in a bacterial cell, despite the relatively short DNA length, have the potential to become much more entangled than human chromosomes.

Bacteria therefore require mechanisms to ensure segregation of their duplicate chromosomes, which may include chromosome condensation mechanisms including DNA looping (self-tethering) and supercoiling [37], both of which are capable of generating lengthwise condensation if suitably regulated. The lengthwise condensation necessary to ensure segregation of duplicate chromosomes can be computed from (14) to be $\lambda_e \approx (\langle \mathrm{Ca}^2 \rangle_0 / \langle \mathrm{Ca}^2 \rangle_\lambda)^{1/3} \approx (10^3/0.1)^{1/3} \approx 20$. According to this estimate, a higher degree of condensation is necessary to ensure segregation of bacterial chromosomes than in the human case; of course, note that the estimate of condensation for bacteria is for DNA, while the previous section's estimate for human chromosomes started with chromatin fiber which is already strongly lengthwise-condensed relative to naked DNA.

Recent experiments do indeed suggest that the bacterial chromosome is highly lengthwise-condensed [38]; mechanisms for this include highly clustered distributions of chromosomal proteins found in chromosome-wide protein-mapping experiments [39]. In addition to lengthwise condensation the cylindrical geometry of many bacterial cells may play a role in promotion of chromosome segregation [8, 40].

5 Conclusions

This paper has presented scaling theories, substantiated by numerical simulations, for equilibrium Ca and Wr for polymers confined within a spherical pore (Sect. 2). A simple scaling description of the results allows equilibrium Ca or Wr to be easily estimated for a wide variety of situations. A general feature of the results is that thermal equilibrium average values of Ca^2 and Wr^2 are rather small despite their crowding in a pore; for example for two polymers with excluded volume, $\langle \mathrm{Ca}^2 \rangle < 0.01N$ even for $2N/R^3 \approx 1$ (Fig. 3). The numerically small prefactors of the scaling laws discussed in this paper are similar to the small prefactors

observed for scaling laws of catenation of tethered polymers [15]; each unit of Ca requires many ($\gg 1$) segments under most circumstances.

It is worth noting that the scaling law proposed here for the catenation of isolated self-avoiding polymers in spherical confinement, (10), has not yet been tested numerically.

Previous results concerning writhes of confined polymers can be understood in terms of the results of this paper. First, work of Micheletti et al. [23] showed that $|\mathrm{Wr}| \approx N^{3/4}$ for ideal polymers inside a pore of radius $R = 4.4$; the value of N/R^3 in that study ranged from 0.64 to 2.8 over $N = 50$ to 250. Referring to Fig. 2(b), over that N/R^3 range, $\langle \mathrm{Wr}^2 \rangle / N$ is in the crossover between isolated and confined regimes, with the result that $\langle \mathrm{Wr}^2 \rangle / N \approx N^{1/2}$. Therefore, over this range, a log-log plot of $\langle \mathrm{Wr}^2 \rangle$ versus N would have a slope near 3/2, explaining the power law observed by Micheletti et al. [23].

Results of Baiesi et al. for $|\mathrm{Wr}|$ of collapsed polymers (polymers in bad solvent) can also be understood in terms of the results of this paper, but now in terms of the scaling function describing $\langle \mathrm{Wr}^2 \rangle$ for polymers with excluded volume, Fig. 3. Baiesi et al. observed that $|\mathrm{Wr}| \approx N^{0.6}$ in bad solvent, for N from 200 to 1000. For the collapsed polymers, $\phi = N/R^3$ will be nearly constant, with $R \approx N^{1/3}$; Fig. 3 indicates that $\langle \mathrm{Wr}^2 \rangle / N$ should be nearly constant in this case, suggesting $\langle \mathrm{Wr}^2 \rangle \approx N^{1/2}$. However, there can be expected to be a gradual increase in net ϕ as $N \to \infty$ due to gradually decreasing surface blob effects. Thus based on Fig. 3, one can expect $|\mathrm{Wr}| \approx N^{\alpha}$ where α is slightly larger than 0.5, as observed by Baiesi et al. [24].

A byproduct of the scaling theory for Wr scaling is description of a writhe instability for a polymer driven by a field coupled to Wr (Sect. 3). A first-order-like transition was observed, similar to the scenario described by Moroz and Kamien [25]. Since this general type of theory has been used as a description of DNA supercoiling [41] it is interesting to see that such a model leads to a highly knotted and writhed state with $|\mathrm{Wr}| \sim N^2$. The writhe-collapsed state with $|\mathrm{Wr}| \sim N^2$ is distinct from the $|\mathrm{Wr}| \approx N$ unknotted plectonemic supercoiled state, which is the equilibrium for a circular polymer under torsional stress only in the case where knot type is constrained to unknot [42].

Experimentally achieving the superwrithed state described in Sect. 3 would require maintenance of torsional stress in DNA, while allowing knotting topology to change. It would be of interest to study the nature of writhe-condensed polymer conformations generated in the case of a semiflexible polymer instead of the freely-jointed polymer studied here. Notably, similar high-writhe states have been observed in numerical calculations for semiflexible polymers under torsional stress where knot type is not controlled [42].

A second mechanism that might be able to drive a writhing instability is cholesteric interactions between nearby segments that prefer local chiral packing. Tight confinement of polymers with cholesteric interactions has been observed to generate chirally wound conformations and enhanced chiral knotting in simulations [43]. This effect provides an explanation for experimental observations of chiral knotting of DNA expelled from viral capsids [44]. It may be useful to understand the relation between the chiral self-organization observed in those studies and the writhe-torque-driven collapse of Sect. 3.

One of the applications of the theory developed in this paper is description of entanglement of chromosomes inside cells (Sect. 4). To simplify the discussion of this, results for circular polymers have been used, but one should keep in mind that the chromosomes of eukaryotes (and some bacteria) are generally linear. Definition of Ca for linear polymers can be made by joining the end segments by a straight line; this construction will in general generate a subleading contribution to Ca, since only $R \ll N$ monomers are needed to make the closure, generating at most a correction $\approx R$ to $\langle \mathrm{Ca}^2 \rangle$. Since $\langle \mathrm{Ca}^2 \rangle \approx N/n \gg R$ under most circumstances (recall $nN \approx R^3$ for reasonably concentrated polymers) the closure

correction is fairly small. Therefore Ca for linear polymers is reasonably well defined, and the scaling results of this paper provide a useful estimate of entanglement even for linear chromosomes.

It is to be emphasized that other mechanisms may well help drive disentanglement of chromosomes in cells. As mentioned above, kinetic effects may limit the degree to which entanglements of separate chromosomes are able to form during interphase (including immediately following cell division) [7]. In addition, it is known from simulation studies that loop structures and heterogeneity of effective segment size along confined polymers [45, 46] generate spatial self-organization and segregation effects, providing potential mechanisms for the observed compartmentalization of the interphase nucleus. It has also been suggested that constraints on topoisomerase activity on chromatin fibers might tend to maintain chromosomes in spatially segregated territories during interphase [47].

All of these effects (and more not yet characterized by experimentalists or imagined by theorists) may play a role in spatially organizing the interphase nucleus, and in reducing overlap of separate chromosomes during interphase. However, the fact remains that following DNA replication, large numbers of remnant catenations of duplicate chromatids plus entanglements between different chromosomes must be resolved before chromosomes can be segregated. The condensation-resolution mechanism discussed in Sect. 4 provides a simple explanation of how this can be accomplished: lengthwise condensation, presumably driven in part by condensin complexes, in concert with topology change mediated by topo II, can drive entanglements out of chromosomes (including initially tightly interwound chromosomes, see Ref. [15]). The estimates of Sect. 4 indicate the degree of lengthwise condensation required to ensure that chromosomes fully separate from one another.

A final comment regarding disentanglement via lengthwise condensation regards the question of the reduction of entanglement entropy apparent during the process described in Sect. 4. There is no doubt that the entropy of the topology of polymers is driven down by this process, which might strike one as paradoxical since $\langle \mathrm{Ca}^2 \rangle_\lambda$ is a thermodynamic average. One should keep in mind that there is no paradox since the polymer is being folded up in a rather precise fashion, by local contraction and thickening. The interactions driving lengthwise condensation (e.g., local folding of chromatin by SMC protein complexes [35]) involve far more energy (in excess of $k_B T$ per segment) than the free energy change associated with freezing out entanglements.

Acknowledgements This work was supported by NSF Grants DMR-0715099, PHY-0852130, DMR-0520513 and MCB-1022117, and by NIH Grant 1U54CA143869-01 (NU-PS-OC). We acknowledge staff and instrumentation support from the Center for Structural Biology at Northwestern University. Support from the R.H. Lurie Comprehensive Cancer Center of Northwestern University to the Structural Biology Facility is acknowledged.

References

1. Doi, M., Edwards, S.F.: Theory of Polymer Dynamics. Oxford University Press, London (1987)
2. de Gennes, P.G.: Scaling Concepts in Polymer Physics. Cornell University Press, Ithaca (1985)
3. Hirano, T.: Trends Biochem. Sci. **20**, 357–361 (1995)
4. Alexandrov, A.I., Cozzarelli, N.R., Holmes, V.F., Khodursky, A.B., Peter, B.J., Postow, L., Rybenkov, V., Vologodskii, A.V.: Genetica **106**, 131–140 (1999)
5. Marko, J.F., Siggia, E.D.: Mol. Biol. Cell **8**, 2217–2231 (1997)
6. Marko, J.F.: Chomosom. Res. **16**, 469–497 (2008)
7. Rosa, A., Everaers, R.: PLoS Comput. Biol. **4**, e1000153 (2008)
8. Jun, S., Wright, A.: Nat. Rev., Microbiol. **8**, 600–607 (2010)
9. Meyer, K.N., Kjeldsen, E., Straub, T., Knudsen, B.R., Hickson, I.D., Kikuchi, A., Kreipe, H., Boege, F.: J. Cell Biol. **136**, 775–788 (1997)

10. Wang, J.C.: Q. Rev. Biophys. **31**, 107–144 (1998)
11. Vologodskii, A.V., Lukashin, A.V., Frank-Kamenetskii, M.D.: J. Exp. Theor. Phys. **67**, 1875–1885 (1974)
12. Frank-Kamenetskii, M.D., Vologodskii, A.V.: Usp. Fiz. Nauk **134**, 641–673 (1981)
13. Otto, M., Vilgis, T.A.: Phys. Rev. Lett. **80**, 881–884 (1998)
14. Everaers, R.: New J. Phys. **1**, 12–54 (1999)
15. Marko, J.F.: Phys. Rev. E **79**, 051905 (2009)
16. Tanaka, F.: Prog. Theor. Phys. **68**, 148–163 (1982)
17. Tanaka, F.: Prog. Theor. Phys. **68**, 164–177 (1982)
18. Müller, S., Schäfer, L.: Eur. Phys. J. B **2**, 351–369 (1998)
19. Baiesi, M., Orlandini, E., Stella, A.L.: Phys. Rev. Lett. **87**, 070602 (2001)
20. Fuller, F.B.: Proc. Natl. Acad. Sci. USA **68**, 815–819 (1971)
21. Orlandini, E., Whittington, S.G.: Rev. Mod. Phys. **79**, 611–642 (2007)
22. Panagiotou, E., Millett, K.C., Lambropoulou, S.: J. Phys. A **43**, 045208 (2010)
23. Micheletti, C., Marenduzzo, D., Orlandini, E., Sumners, D.W.: J. Chem. Phys. **124**, 064903 (2006)
24. Baiesi, M., Orlandini, E., Whittington, S.G.: J. Chem. Phys. **131**, 154902 (2010) (2009)
25. Moroz, J.D., Kamien, R.D.: Nucl. Phys. B **506**, 695–710 (1997)
26. Brereton, M.G., Shah, S.: J. Phys. A **13**, 2751–2762 (1980)
27. Brereton, M.G., Shah, S.: J. Phys. A **14**, L51–L54 (1981)
28. Ferrarri, F., Kleinert, H., Lazzizzera, I.: Phys. Lett. A **276**, 31–36 (2000)
29. Otto, M.: J. Phys. A **34**, 2539–2547 (2001)
30. Marko, J.F., Siggia, E.D.: Phys. Rev. E **52**, 2912–2938 (1995)
31. Uemura, T., Ohkura, H., Adachi, Y., Morino, K., Shiozaki, K., Yanagida, M.: Cell **50**, 917–925 (1987)
32. Adachi, Y., Luke, M., Laemmli, U.K.: Cell **64**, 137–148 (1991)
33. Anderson, H., Roberge, M.: Cell Growth Differ. **7**, 83–90 (1996)
34. Giménez-Abián, J.F., Clarke, D.J., Devlin, J., Giménez-Abían, M.I., De la Torre, C., Johnson, R.T., Mullinger, A.M., Downes, C.S.: Chromosoma **109**, 235–244 (2000)
35. Hirano, T., Mitchison, T.J.: Cell **79**, 449–458 (1994)
36. Ono, T., Losada, A., Hirano, M., Meyers, M.P., Neuwald, A.F., Hirano, T.: Cell **115**, 109–121 (2003)
37. Trun, N., Marko, J.F.: ASM News **64**, 276–283 (1998)
38. Wiggins, P.A., Cheveralls, K.C., Martin, J.S., Lintner, R., Kondev, J.: Proc. Natl. Acad. Sci. USA **107**, 4991–4995 (2010)
39. Vora, T., Hottes, A.K., Tavazoie, S.: Mol. Cell **31**, 247–253 (2009)
40. Jun, S., Mulder, B.: Proc. Natl. Acad. Sci. USA **33**, 12388–12393 (2006)
41. Bouchiat, C., Mézard, M.: Phys. Rev. Lett. **80**, 1556–1559 (1998)
42. Vologodskii, A.V., Marko, J.F.: Biophys. J. **73**, 123–132 (1997)
43. Marenduzzo, D., Orlandini, E., Stasiak, A., Sumners, D.W., Tubiana, L., Micheletti, C.: Proc. Natl. Acad. Sci. USA **106**, 22269–22274 (2009)
44. Arsuaga, J., Vazquez, M., McGuirk, P., Trigueros, S., Sumners, D., Roca, J.: Proc. Natl. Acad. Sci. USA **102**, 9165–9169 (2005)
45. de Nooijer, S., Wellink, J., Mulder, B., Bisseling, T.: Nucleic Acids Res. **37**, 3558–3568 (2009)
46. Cook, P., Marenduzzo, D.: J. Cell Biol. **186**, 825–834 (2009)
47. Dorier, J., Stasiak, A.: Nucleic Acids Res. **37**, 6316–6322 (2009)